The LVD tracking system chambers

Anzivino, G.; Benvenuto, P.; Bianco, S.; Casaccia, R.; Dulach, B.; Fabbri, D.; Fabbri, F.L.; Gatta, M.; Giardoni, M.; Laakso, I.

Published in:
Nuclear Instruments and Methods in Physics Research Section A Accelerators Spectrometers Detectors and Associated Equipment

DOI:
10.1016/0168-9002(93)91288-X

Publication date:
1993

Nuclear Instruments and Methods in Physics Research A329 (1993) 521–540
North-Holland

NUCLEAR
INSTRUMENTS
& METHODS
IN PHYSICS
RESEARCH
Section A

The LVD tracking system chambers

G. Anzivino, P. Benvenuto, S. Bianco, R. Casaccia, B. Dulach, D. Fabbri, F.L. Fabbri, M. Gatta, M. Giardoni, I. Laakso †, M. Lindozzi, L. Passamonti, V. Russo, S. Sarwar, G. Sensolini, M. Ventura, L. Votano and A. Zallo
INFN - Laboratori Nazionali di Frascati, P.O.Box 13, I-00044 Frascati, Roma, Italy

D. Mencarini
Università di Bologna, e Sezione INFN, Via Irnerio 46, I-40126, Bologna, Italy

E. Pallante
Università di Roma I "La Sapienza", P.le Aldo Moro 2, I-00185, Roma, Italy

Z. Aftab, M.M. Ali, K. Chen, R. Chen, S. Cong, X. Cui, H. Ding, B. Gao, Y. Li, L. Lu, B.K. Minhas, Z. Shi, A.R. Shah, Y. Sun and X. Zhou
ICSC World Laboratory, Lausanne, Switzerland

Received 5 November 1992

1. Introduction

The LVD detector [1] can be defined as an underground observatory with the main objectives of studying neutrinos from stellar collapse and searching for point-like sources of gammas and neutrinos of very high energy. This multipurpose apparatus is being installed in hall A of the Gran Sasso Laboratory [2] at a vertical depth of 3600 m.w.e. It consists of a large volume of liquid scintillator divided into modules and of a tracking system made of layers of streamer tubes. The detector design fulfils the following aims:

– the study of the neutrino interactions inside the detector with energy measurement for low-energy neutrino interactions, and pattern identification for higher energy events;

– the detection of passing muons with track reconstruction, up–down discrimination and time of flight measurement.

The apparatus consists of 190 basically identical modules. Each module comprises 9.6 t of liquid scintillator divided into eight modular counters and an L-shaped tracking chamber, containing a double layer of streamer tubes and facing the bottom and one vertical side of the module. These modules are inserted into an iron support structure. The whole array, which measures $40 \times 12 \times 13$ m^3, is divided longitudinally into five identical towers. The total weight, including 1824 tons of liquid scintillator, the tracking system and the support structure, is 3600 t. Fig. 1 shows a detailed view of a few LVD modules.

2. The tracking system

Each of the five longitudinal towers of the tracking system consists of eight horizontal and five vertical double layers of limited streamer tubes (LST) totalling about 15 000. The geometrical acceptance of the detector is 7559 m^2 sr for an isotropic flux and reduces to 6024 m^2 sr if it is required that particles cross three ideally continuous planes. The basic element of the design of the tracking system is the L-shaped chamber fastened to the iron box containing the liquid scintillator detectors. There are 80 large and 110 small chambers, housing respectively 84 and 72 LSTs, placed so as to form the eight horizontal and the five vertical planes (fig. 2) and to facilitate passage along the longitudinal corridors; larger (1.4 m) corridors run between each tower. Each streamer tube layer is equipped with a

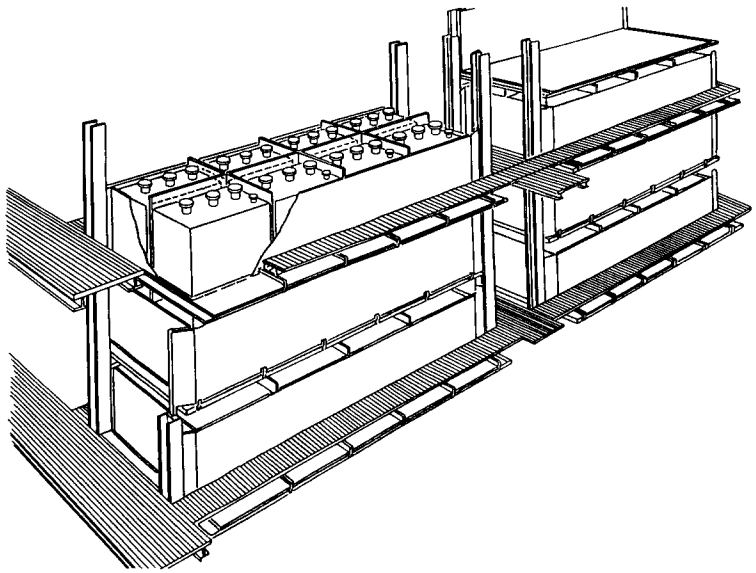

Fig. 1. A detailed view of a few LVD modules.

digital readout in two coordinates, and the signal is picked up by 3.8 cm wide strips, parallel (X-strips) and transverse (Y-strip) to the streamer tubes. Y-strips run continuously from the horizontal to the vertical side of the chamber. Signals from pick-up strips are discriminated and fed into shift registers. A serial readout is then performed by a CAMAC processor. The complete tracking system totals about 82 000 channels.

Since the spatial resolution on the X and Y coordinates is 1.1 cm, the intrinsic angular resolution of the apparatus is expected to be $\sim 0.1°$.

The angular resolution has been evaluated taking also into account the effect of the multiple scattering in the propagation of muons into the apparatus [3]. For this purpose, using Monte Carlo simulation based on the GEANT package, 10 000 muons were uniformly generated and tracked through the apparatus with a fixed angle of 45° with respect to the zenith, 5–500 GeV of energy range, and without generation of secondary particles. In the reconstruction of the track, we then took into account the spatial resolution and imposed a reasonable trigger condition, i.e. at least three hit strip planes (the OR of the two layers is defined as a plane) and one hit scintillator counter are required. The plot of the angular resolution is shown in fig. 3 as a function of the muon energy.

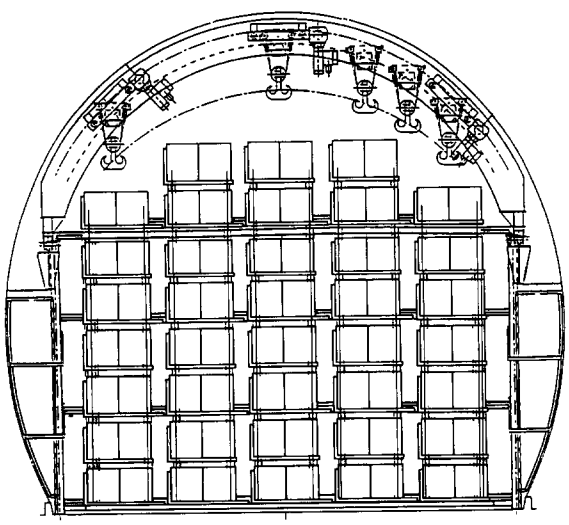

Fig. 2. Cut-away view of the LVD apparatus.

The angular resolution of the apparatus is clearly dominated by multiple scattering in the liquid scintillator up to $E_\mu \leq 10$ GeV, is sensitive to it up to ~ 50 GeV and has an asymptotic value $\sim 0.1°$ in the 50–500 GeV interval, where the spatial intrinsic resolution of the apparatus dominates, in the absence of other systematic effects. Moreover, the average muon energy at the level of the detector is ~ 300 GeV, corresponding to a energy threshold of 2.1 TeV at the surface. Since the mean deflection at these energies is ~ 4 mrad due to multiple scattering in the rock, we can conclude that the apparatus has an angular resolution for energies greater than 50 GeV mainly determined by the effect of multiple scattering in the rock.

2.1. The mechanics and the chamber assembly

The design of the modular tracking chamber fulfils many objectives:

– support of the double layer of LSTs with the right planarity, while hooked to the iron module;

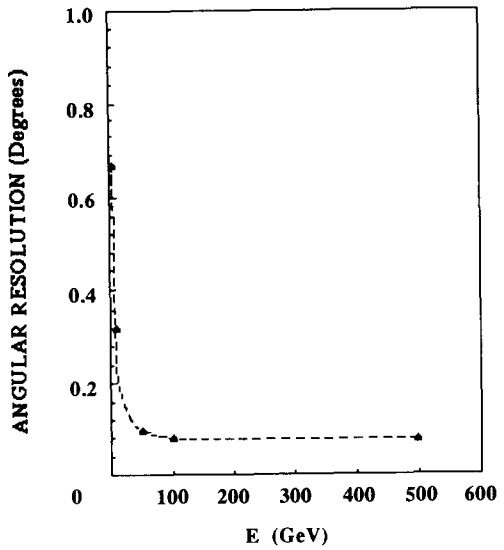

Fig. 3. The angular resolution as a function of the muon energy in the range 5–500 GeV.

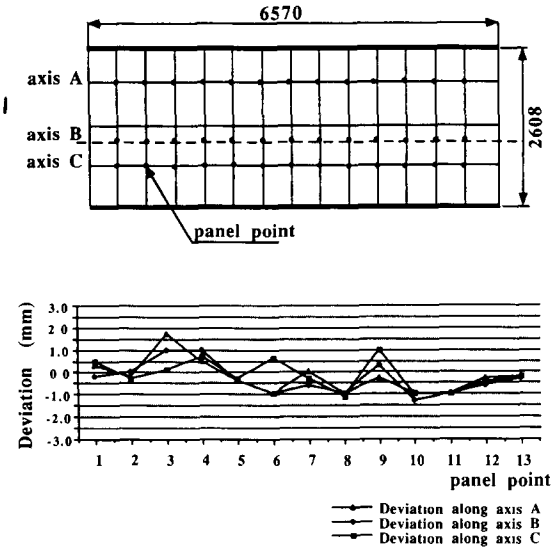

Fig. 4. Planarity measurements on a wide panel.

– room for front-end electronics, gas piping, high-voltage and signal cabling;

– fast and easy assembly of all the components, with the possibility of substituting parts, including the streamer tubes;

– continuity of the transverse *Y*-strips between the horizontal and the vertical planes;

– stability of components and assembly over ten years;

– use of materials with low radioactivity (less than 0.5 Bq/kg);

– low cost.

The solution adopted is a mechanical structure composed of two metal panels, one vertical and the other horizontal, joined at an angle of 90° by means of hinges to permit adjustments during assembly.

The coupling to the iron module is made with adjustable supports on the longitudinal edges of the horizontal and vertical panels. Three different dimensions of metal panels have been adopted: a common vertical panel ($6570 \times 1085 \times 37$ mm^3) that can be connected either to a large horizontal panel ($6570 \times 2607 \times 37$ mm^3) or to a small horizontal one ($6570 \times 2096 \times$

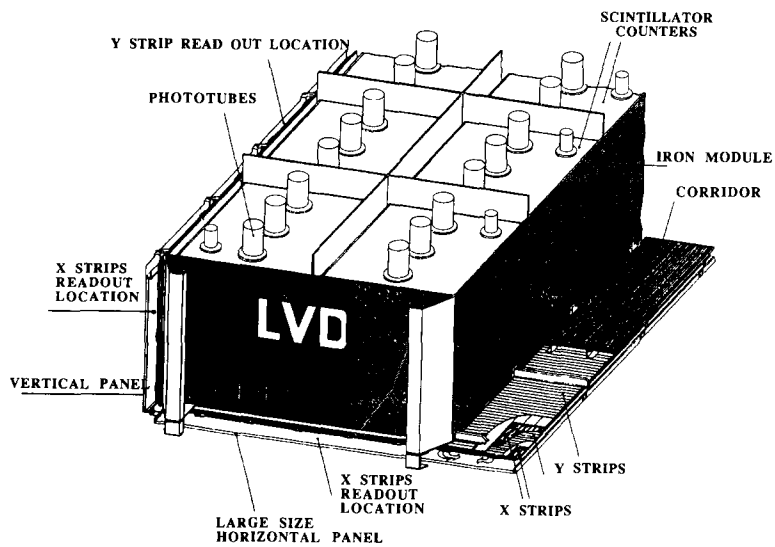

Fig. 5. A view of the assembled chamber together with the iron module and the scintillator counters.

37 mm^3). Each panel consists of a tubular iron frame covered on both sides by a 1 mm thick sheet of iron fixed with rivets and glue (a composite type CIBA AW106 + HV 953U). All the surfaces (tubes and sheets) are zinc-coated. The design adopted guarantees a total planarity of 3 mm and dimensional tolerances of 1 mm. The materials used have been tested for radioactivity content, giving repetitive results well inside the acceptable limits.

Flexure and planarity tests have been made on the first prototype to ascertain the conformity with the design specifications. For the flexure tests, the panel was supported along its length, in correspondence to the points of connection with the iron module, and a load of 40 kg/m^2 (30% greater than the operational load) was distributed uniformly on the surface. The flexion measured along the panel centre line, in correspondence to the supports and in between them is lower than 2.5 mm. The wide horizontal panel was used to test the planarity which, as shown in fig. 4, is better than 3 mm.

Fig. 5 shows the assembled chamber together with the iron module and the scintillator counters. The gas piping and the local high voltage distribution cables are housed on one side of the chamber, the front-end electronics of the *X*-strips on the other one. Since the streamer tubes placed on the horizontal and vertical panels share common *Y*-strips, the latter are thermally bent at an angle of 90° and the front-end electronics for them is placed in a U-shaped iron beam, attached along the length of the vertical panel. The stratigraphy of the assembled module is as follows: above the iron panel an insulating plane is placed, then the two layers of streamer tubes staggered by 1.5 cm, each one with its pick-up strips parallel and transverse to the wires, finally the last insulating plane. These planes are made of a 1 mm layer of PVC with a 40 μm Al sheet glued on the internal side to provide a continuous equipotential ground plane for the facing pick-up strips. The LSTs, in groups of four, are inserted in PVC jackets, with the upper coverless side facing the *Y*-strips. The use of the jackets not only allows the substitution of the streamer tubes in the case of malfunctioning but facilitates the construction of the chamber and its handing over to industry, since the first mechanical assembly can proceed without the LSTs. All the components are assembled making use of the double-face tape (3M VHB9473).

An overall precision on the alignment of the order of a few mm is reached by using a set of appropriate reference marks during the component assembly. This set is also used for the alignment of the module when the apparatus is in its final position. The link to the iron module housing scintillator detectors is easy and quick and is made just before the installation of the whole module in the apparatus structure.

3. The detector

3.1. The limited streamer tubes

The LVD streamer tubes are the standard Frascati coverless plastic tubes [4] (6.3 m long) and operate in limited streamer mode. A PVC extruded profile, containing eight rectangular cells with a 1 cm^2 cross section, is internally coated with graphite paint. The surface resistivity of the graphite coated cathode (0.08–2 MΩ/□) is well within the transparency limits. Cu–Be silver plated anode wires, with a diameter of 100 μm, are strung through the centre of each cell and supported every 50 cm by plastic bridges. The profiles are enclosed by a PVC envelope, and plastic caps welded at the ends provide the electrical and gas connections. The limited streamer tubes are filled with a binary gas mixture of argon (25–30%) and isobutane (75–70%). To provide the 15 000 LSTs needed for the experiment, two production lines have been used: one at Frascati INFN National Laboratory and the other at Houston University. In order to guarantee good reliability and long lifetime, a quality selection of streamer tubes has been performed on the basis of a long-term acceptance test in the ASTRA (Advanced Streamer Tube and Test Research Apparatus) experiment facility established at the Frascati laboratory, where current monitoring of each tube is performed at high voltage (4.9 kV) for a period of four weeks. The selection criteria and test results are reported elsewhere [5]. In order to correctly choose the operational point and guarantee its stability, detailed studies on the performance of the LST have been performed: the transition between the proportional regime and streamer regime as a function of different percentages of Ar:C_4H_{10} gas mixture, high voltage and temperature [6] has been investigated; a comparison has been made between the use of a standard binary and a low-hydrocarbon ternary gas mixture, and the effect of gas impurities on chamber performance has been studied [7]. All the results presented in this paper refer to modules assembled using LSTs produced at the Frascati tube factory and selected in ASTRA.

3.2. Pick-up electrodes

The pick-up electrodes or strips for the LSTs consist of a sandwich of Al–PVC–Al. The aluminium sheets are 40 μm thick, 38 mm wide, and are thermally glued on both sides of the 1.6 mm thick PVC sheet. Two parallel *X*-strips cover one LST. This width was chosen as a compromise between the required angular resolution and the number of electronic channels economically feasible. Individual strips are made in groups, each group consisting of eight Al strips on one side of the PVC and a continuous Al sheet (acting as ground

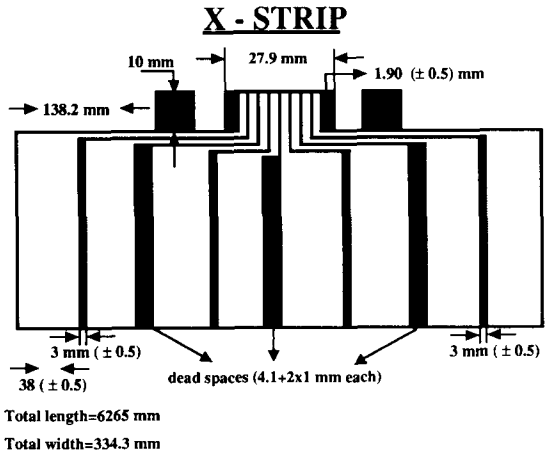

Fig. 6. X-strip design at the connector side.

plane) on the other. The distance between individual strips is 3 mm for X-strips and 1.5 mm for Y-strips. Each group of eight strips tapers on the signal side where it is shaped like a standard gold-plated edge connector (fig. 6). The milling and gold-plating technique for the strips was developed at Perugia University [8], and all the LVD strips are produced there. The design of the strips is the result of the optimization of the induced signal collection; it accomplishes the best possible match between the characteristic impedance of the strip ($Z \sim 10\ \Omega$) and the input impedance of the commercially available front-end electronics (SGS Company) and minimizes the cross-talk between the individual strips.

Tests were carried out to measure the cross-talk in the final strip–flat-cable–front-end electronic configuration of the chamber. Two adjacent strips were connected to different front-end cards, set to the same threshold. One of the strips was pulsed with a signal that simulated the wire induced signal. The pulse height was adjusted to reach the value of the threshold, then was increased until the same 50% efficiency was obtained, by cross-talk, on the card connected to the adjacent strip. The ratio of the two pulse heights defines the cross-talk. It was found to be less than 1% for X-strips and of the order of 2–3% for the Y-strips. We can conclude that the electromagnetic coupling cross-talk between strips and flat cable is negligible when compared with the expected multihit due to the coupling between the LST wires and the strips, as we shall see later.

3.3. HV network

The pulse propagation mechanism on the streamer tube device with the resistive cathode and external pick-up strips orthogonal and parallel to anode wires has been well described elsewhere [9,10]. Due to the streamer tube length and the characteristics of the streamer pulse duration, wire and strips behave as transmission lines.

In the case of the X-strips, two different transmission lines can be identified: one between wires and strip and another between strip and ground. When a streamer is formed, the distortion of the electrical field between the anode and the resistive cathode first excites the transmission line wire-strip, and when the current generated reaches one end of the line, it is injected in the strip-ground line. Since the high impedance cathode does not interfere very much with signal transmission, strip signals are the image of wire signals and are thus affected by the load resistance of the wire-ground line. In the orthogonal strips, the pulses of the wire-ground and strip-ground lines travels simultaneously and independently. Fig. 7 shows the HV network adopted for the LVD LSTs. Individual wires are terminated on their characteristic impedance with 220 Ω resistors and connected to the HV power supply through a current limiting 10 MΩ resistor.

The values for capacitor C_g and resistor R_{out} have been carefully choosen in order to have the best compromise between the optimization of the strip readout efficiency and the minimization of the multihit on parallel strips. This can be understood if we recall that the LVD parallel strips cover four wires of one LST. In fact, in the absence of a capacitor with respect to ground, the current loop shuts off through the parallel of the other seven wires. Due to the high impedance toward the HV line, the current injected in one wire and flowing through it, is reinjected in the neighbouring wires, approximately 1/7 per wire of the total current generated. Due to the capacitive coupling

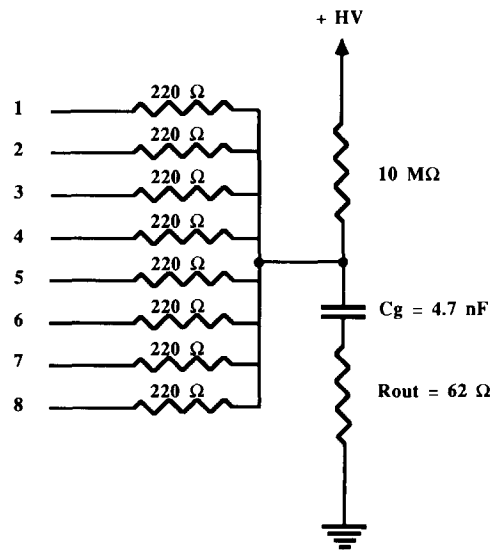

Fig. 7. The high voltage network scheme.

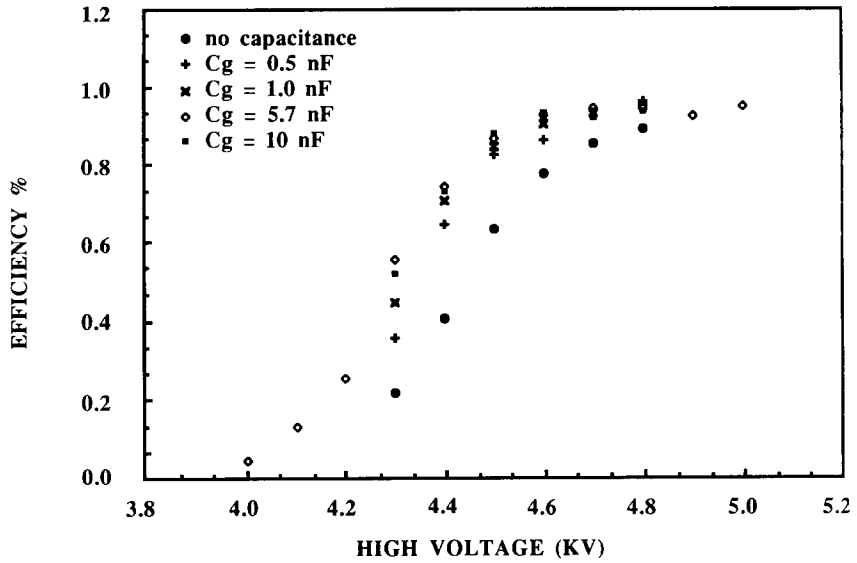

Fig. 8. The X-strip efficiency for different values of C_g.

wire-strip, a negative signal will be induced on the strip and, in our case, each strip will have a positive signal induced by the hit wire and three negative signals induced by the three adjacent ones facing the same strip, with a consequent lowering of the signal. On the other hand, this effect is responsible for the lowering of strip multihit. As one wire is struck, due to the local direct charge induction, the nearby strip, too, has a positive signal that will sum with the negative signal described above. As a consequence, the probability that more than one strip has a signal for one wire hit decreases. The optimum balance between the two effects can be obtained using a C_g greater than the wire capacitance and tuning the value of the resistor to minimize the strip multihit. For this purpose, a test was performed for our LSTs and strips. The two parallel strips facing one LST were connected with one front-end card on the HV side. The response from the OR of the eight wires and from the digital OR output of the front-end card was recorded. An independent trigger was provided by a cosmic ray telescope of plastic scintillators. The gas was a 30:70 $Ar:C_4H_{10}$ mixture. Fig. 8 shows the strip efficiency with respect to the scintillator trigger varying C_g, with $R_{out} = 50\ \Omega$ and the reference level of the electronic threshold (see section 4.1) set at 60 mV. The importance of the presence of C_g is clearly seen, as well as the saturation effect as soon as its value exceeds the wire capacitance.

In order to choose the R_{out} value, a test was carried out using a specially built LST in which only four wires are connected in parallel, while the others four can be connected to the HV independently. It was possible to separate the contribution of each of the wires facing one strip on the nearby strip of the same LST. When only wire 4 (fig. 9) is connected to HV the multihit probability, defined as the ratio between the number of counts of strip A to the number of counts of strip B, varies from 60% for $R_{out} = 50\ \Omega$ to 40% for $R_{out} = 150\ \Omega$; while full efficiency is kept until R_{out} is 100 Ω (test conditions are: wire HV 150 V above the knee and the reference level of the electronic threshold set at 30 mV).

3.4. The gas distribution system

The gas distribution to the chambers is obtained by means of two L-shaped stainless steel manifolds (2.5 cm^2 cross section) fixed on the metal panels on the high voltage side. Pairs of LSTs, one of the upper layer and one of the bottom, are connected in parallel to the gas manifold. Since the tubes present a negligible impedance to gas flow, even small variations of the connection impedance can cause an unacceptable flow rate variation through parallel connected LSTs. A homogeneous flow is achieved by inserting an impedance

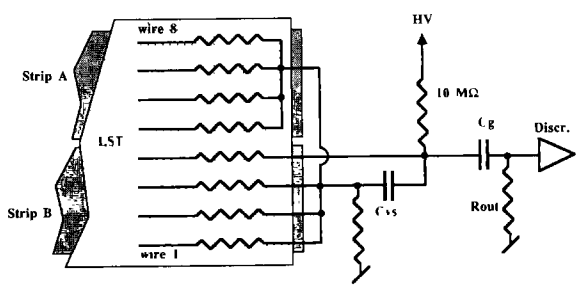

Fig. 9. Special LST setup.

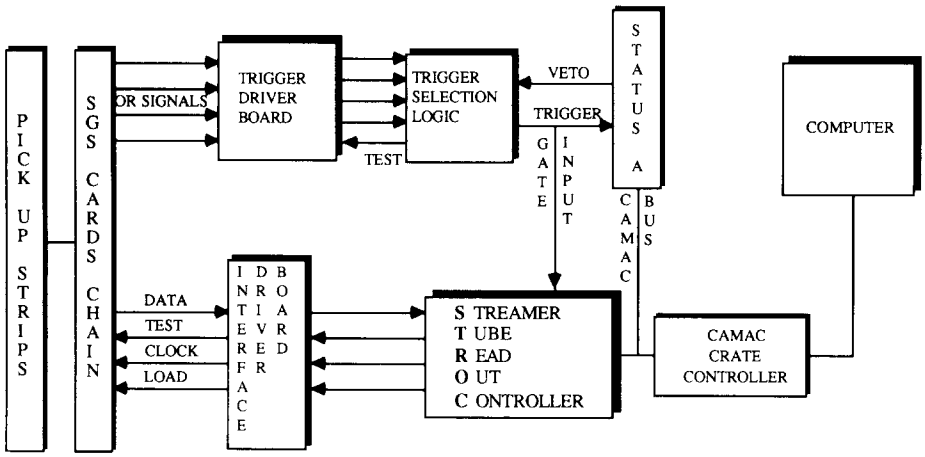

Fig. 10. The block diagram of the readout system for the tracking chambers.

(a steel cylinder having a helicoid groove) in series at the output of each pair of tubes. The overpressure due to this impedance, measured on different positions in the chamber, is (0.5 ± 0.1) mbar/l h^{-1}, for a flow rate corresponding to one volume change each 12 h. This system also guarantees self-compensation for small gas leaks. Particular attention is devoted to the leakage test during the chamber assembly. This, indeed, is one of the important chamber characteristic to be checked in order to guarantee stable operation and environmental safety, since an inflammable gas mixture is normally used. Leaks must be minimized to prevent the loss of mixture and also to stop the atmospheric impurities from entering the tubes. For our LSTs, the limit value adopted is 2% gas leakage per day in the operational conditions of one volume being recirculated in two days at an internal overpressure less than 10 mbar. In order to guarantee the required leak rate, individual LSTs are tested as soon as they are inserted in the module in their final position. The hermeticity method is used. The tubes are pressurized to 20 mbar and their drop of overpressure is observed for a period of three days. In fact, due to the material deformation of pressurized LSTs, a measurement at a level of a few percent leakage per day sensitivity requires such a long observation in order to overcome the delayed strain of the material. The detailed procedure and the correspondence between the observed tube leakage and the intrusion value expected in the given flow conditions will be described in a forthcoming article. Finally, the

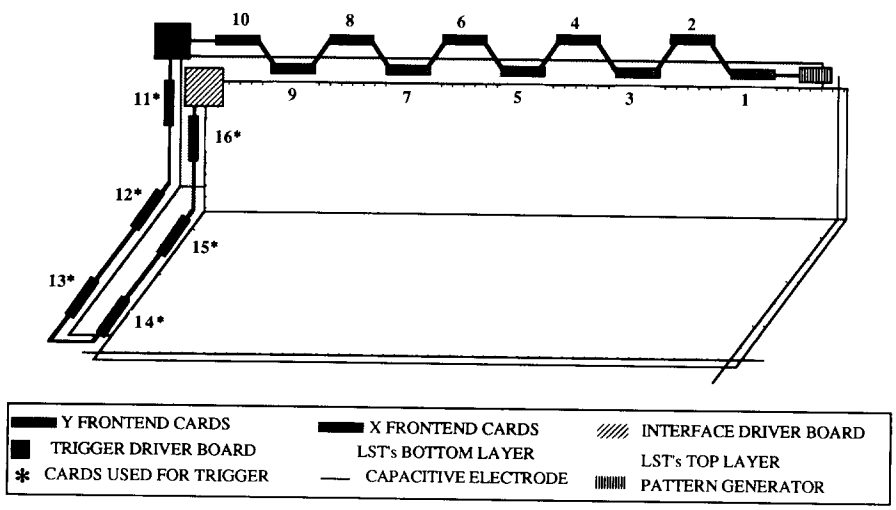

Fig. 11. Readout chain configuration of one chamber.

drop pressure of the whole chamber is also observed for three days in order to check any possible leakage along the connections to the gas manifold.

4. The readout electronics

The block diagram of the readout system for the tracking chambers is shown in fig. 10. Its main functions can be summarized as follows. The signals induced in the strip by the streamer are fed to the inputs of a front-end chain consisting, for one chamber, of 16 electronic cards. When the amplitude of a strip signal exceeds the threshold level at any channel of the card, it generates a digital OR pulse. The digital pulses caused by the signals at any of the four layers of X-strips are sent through a trigger driver board to the experiment trigger selection logic. The STATUS A module checks for a trigger pulse at one of its inputs. When a valid trigger is detected, the STATUS A disables the trigger selection logic by sending a veto signal. Simultaneously, the trigger pulse is sent to the gate input of the CAMAC processor named STROC (streamer tube readout controller [12]), which communicates with the front-end chain through an interface driver board. In response to a trigger signal, the STROC sends a load pulse to all the cards. This signal stores the information present at the inputs in the shift registers of the front-end chain. The STROC reads the information by generating a 5 MHz clock signal that serially shifts the data into its internal memory and performs the zero suppression and the clustering of up to seven adjacent hit channels. The computer receives these data by initiating a standard CAMAC read cycle. At the end of the cycle the trigger is reenabled.

4.1. Chamber readout configuration

The configuration of the readout chain components is shown in fig. 11. SGS INFN-32 type cards are used to pick up the signals from the strips. The card, specially designed to provide an interface for streamer tube detectors, has 32 input channels and consists of eight hybrid integrated circuits (CMOS D779). Each hybrid circuit has four input channels and contains builtin amplifiers, discriminators, one shot multivibrators and a 4-bit shift register. The input impedance of the hybrid circuit is about 25 Ω. The common threshold reference voltage is applied at the input of all the discriminators and can be set locally on board or remotely. This reference value is about a factor of 10 bigger than the actual applied threshold. For convenience we will henceforth refer to this set reference level. For each card the outputs of all the one-shots are ORed together and the duration of the pulse has been adjusted to 2.5 μs. During this interval, a load signal, generated by STROC, latches the level of all the one-shot components into the shift registers of the chain. This information is then read by the controller. All the sixteen cards, needed to read about 500 channels of one chamber, are serially connected in a daisy chain line and signal lines are terminated with 120 Ω resistors at one end. Ten cards are connected to the transverse Y-strips, the remaining six to the parallel X-strips. The digital OR pulses corresponding to the four X-strip layers of the chamber are fed to the trigger driver board. The main function of the board, custom developed, is to form logical OR of the digital pulses generated at the same layer. The board can also control the pulse width of the output signals. The following four ECL signals are sent to the experiment trigger selection logic: V_{up} and V_{down} for the upper and lower layers of X-strips of the vertical panel; H_{up} and H_{down} for the horizontal panel.

The interface driver board is used for communication between the front-end chain and the STROC. The original 8-channel board designed at Padua University [12] was partially modified to meet the specific requirements of the LVD experiment. This board acts as a differential receiver/transmitter for various signals involved in the readout cycle. Direct current power is also supplied to the readout chain through the board. The respective reference level of the threshold voltages for both X- and Y-strips are also set at the board and can be controlled either locally on the board or remotely via DAC module. Different threshold voltages are set for the X- and Y-layers because the strip multihit is not the same at a common threshold value. The board can also be used to supply an external refresh signal to the chain.

The functional status of the readout chain is also checked event by event by a local pattern generator board connected at the end of the chain. A known 16-bit pattern is loaded into it before every readout and shifted through the full chain during the readout cycle. Eight bits in the loaded pattern are used to identify the type and position of a particular chamber.

4.2. Testing of the front-end cards

Since a large number of the front-end cards is required for the LVD experiment (3200), it was considered necessary to have an automatic testing device that can check the characteristics and various functions of the card. For this purpose a microcomputer-based system has been designed that can perform the following three tests:

- threshold test;
- frequency response test;
- shift register test.

In the first one the channel uniformity of the actual threshold is tested for three different threshold values.

The frequency response test determines the maximum input signal frequency at which the card can generate a digital OR pulse with 100% efficiency. The frequency of the input signal is increased in steps of 10 kHz.

In the shift register test, 16 different 4-bit patterns are shifted serially through the card and this is accepted if no errors are detected comparing the received and the sent pattern.

The testing program can be run by a nonspecialist operator and the results of the three tests are displayed, on-line, in graphic form.

4.3. Pick-up strips continuity test

In order to check the electrical continuity and efficiency of the pick-up strips, two capacitive electrodes are coupled to the strip layers of a chamber (fig. 11), one electrode is glued along the longitudinal axis perpendicular to the *Y*-strips, while the other is glued perpendicular to the parallel strips and stretches along the horizontal and vertical planes of a chamber. The electrode (4 mm wide and 1 mm thick) can be treated as a transverse transmission line along the ground plane of the module, with a characteristic impedance of 50 Ω. The readout strips in the transverse direction present a uniform periodic capacitance to this line. These electrodes can be used to test a tracking module without switching on the streamer tubes and to distribute a test pulse signal uniformly to the readout strips.

When the electrodes are pulsed with a 2 V signal having rise and fall times of 10 and 40 ns, respectively, the signal is uniformly distributed to the readout strips, due to the capacitive coupling. The amplitude of the signals on the strips is of the order of 10–20 mV, comparable with the real one. No signal reflections are observed on the readout strips due to termination provided by the readout cards and the inter-strip cross-talk is also negligible. The maximum propagation delay of the test signal is 50 ns, very short as compared to the duration of the 2.5 μs pulse generated at the front-end card. A computer is used to test the readout strips by selecting a trigger from the layer that is being pulsed. This allows easy identification of dead or inefficient channels.

5. Tracking chamber response

Many aspects of the tracking system response have been studied: mainly, operating characteristics of individual streamer tubes inside the chamber and strip readout optimization. The overall performances, such as the efficiency of the system as a function of the applied HV and of the front-end electronic threshold, the spatial uniformity and the tracking resolution, have been measured.

For this purpose a cosmic ray test facility setup, controlled by a MaC-II computer, has been used at Frascati Laboratory. In this setup individual chambers are operated with a 25 : 75 $Ar : C_4H_{10}$ mixture of which the composition and the flow rate are regulated by HI-TECH mass flowmeters, with an accuracy of 1% and a maximum output capacity of 200 $l\,h^{-1}$. The setup is designed to perform tests on the readout system, to record the response from the wires of individual LSTs, and to carry out cosmic ray data acquisition in different trigger conditions.

5.1. LST response

All the LSTs of one chamber are at first flushed with $Ar : C_4H_{10}$ mixture at a flow of one volume change in four hours, and a minimum of five volume changes are carried out before applying high voltage. Although the LSTs, assembled in the chambers have already been selected in the ASTRA facility, we have avoided switching them on again, after a lot of handling or long inactivity, without a new conditioning. In this phase, the voltage applied to the LSTs is increased in sixteen variable steps of the order of 100 V up to 5300 V and then at the end kept at 4900 V. The duration of each step is one hour, with a limiting current of 4 μA. For the conditioning test, we linked the MaC-II with the Caen SYS127 supply system, accessing through its serial line to the conditioning program resident on EPROM.

No tube selection is performed on the bases of the results of the conditioning, but all "live" LSTs pass to next test phase, which consists in measuring count rates from wire signals as a function of the anodic high voltage. The rise of count rate corresponds to the gradual transition between the proportional and the limited streamer regime; in the latter the pulse charge is almost independent of the initial ionization and the count rate is almost constant. The plateau region corresponds to the highest possible efficiency of the detector (~ 92% for normal incidence). In these plateau measurements, wire signals are discriminated at a threshold of −10 mV/50 Ω, for which the transition between the two regimes can be correctly observed. A dead time of 2 μs is applied so as to be able to neglect the afterpulses generated by UV photons (extracting secondary electrons from the cathode) and the multistreamers produced by particles crossing the detector at a small angle with the wire. The voltage is increased from 4000 V up to a value ranging from 5100 up to 5500 V, with a limiting current of 2 μA. Count rates as a function of the anodic voltage are fitted with two lines, one for the transition region, the other for the plateau region. The intersection of the two defines the

position of the knee; we also define a breakdown point as the intersection of the plateau and the discharge region or, when this is not clearly visible, as the last measured point in plateau.

Fig. 12 shows the distribution of the voltages corresponding to the knee and the breakdown point for each LST of one chamber. The knee voltages and the count rate values as a function of the LST position in the chamber are shown in fig. 13. The systematic effect observed in the count rate depends on the different geometrical acceptance of vertical and horizontal LSTs, with respect to the cosmic ray distribution at sea level.

The study of the performances of the LSTs in the real detector situation and their selection on the basis of the single plateau rate are crucial in order to correctly choose the working point and to insure a stable and efficient operation of the tracking system.

In fact, the transition voltage to the streamer regime strongly depends on gas composition, pressure and temperature [6,10]. For instance, impurity gas intruded in the chambers due to leakage affects the efficiency plateau [7]; similarly, fast changes in the atmospheric pressure or temperature gradient. In addition to these effects, which are well described elsewhere, it must taken into account that in the HV distribution scheme foreseen, up to twelve LSTs are fed by one HV channel, with a limiting current of 5 μA. This means a drop of 50 V on the applied voltage, due the 10 MΩ

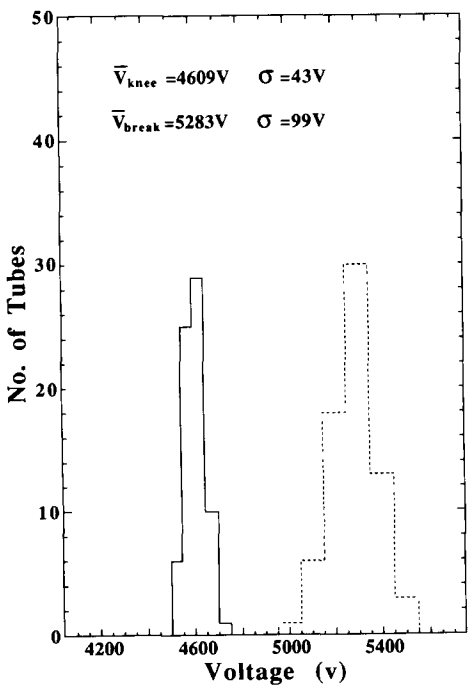

Fig. 12. The distribution of the voltages corresponding to the knee and the breakdown point for one chamber.

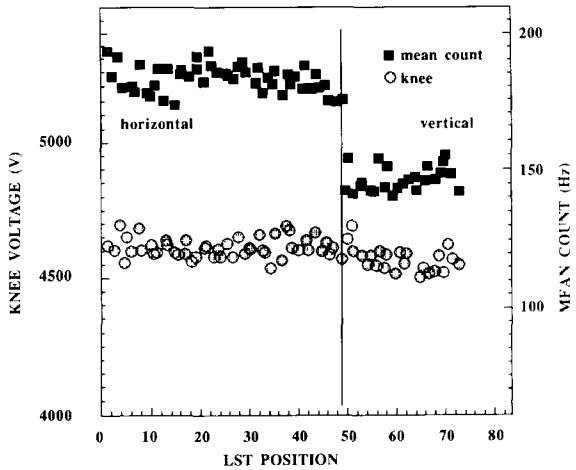

Fig. 13. The knee voltage and count rate distributions as function of the position in the chamber.

resistor. Taking into account all the above considerations, a working point at least 100 V above the knee and a plateau length not less than 350 V seemed reasonable in order to ensure constant efficiency and stable operation of the whole system. In the end we rejected all the tubes without a measurable plateau, either with a plateau length less than 350 V, or with a count rate in the plateau exceeding the mean count on the chamber either by more than 15% or by less than 12% (one missing wire).

5.2. Ground configuration and noise minimization

A great effort has been dedicated right from the beginning to the optimization of ground (signal) configuration and to the study of possible cross-talk between the two layers of LSTs and strips. We have found that

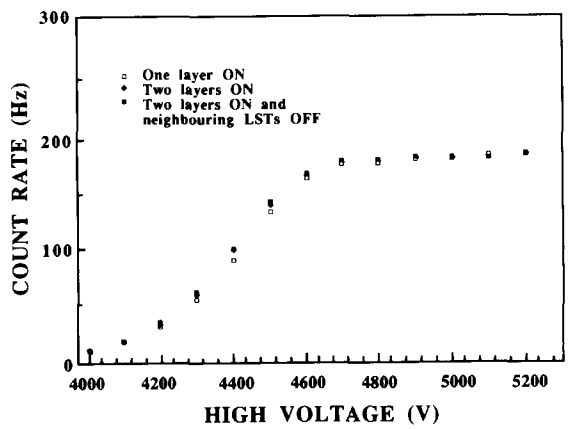

Fig. 14. The plateau from wire signal of one LST in different conditions: (a) with only one layer switched on; (b) both layer switched on; (c) with neighhouring LSTs switched off.

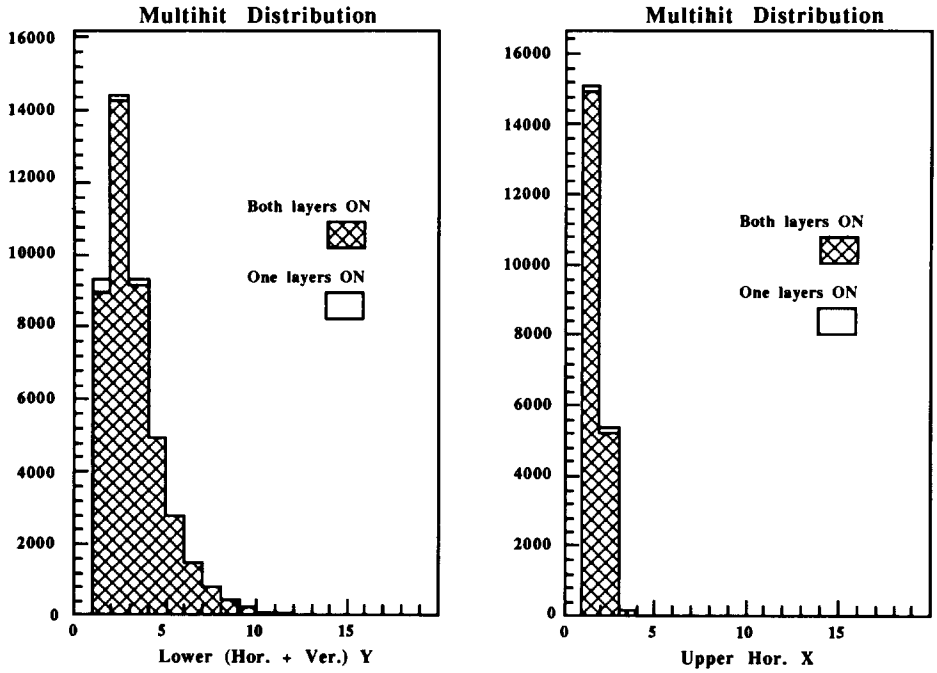

Fig. 15. Multihit distribution in one layer with the other layer switched on or off.

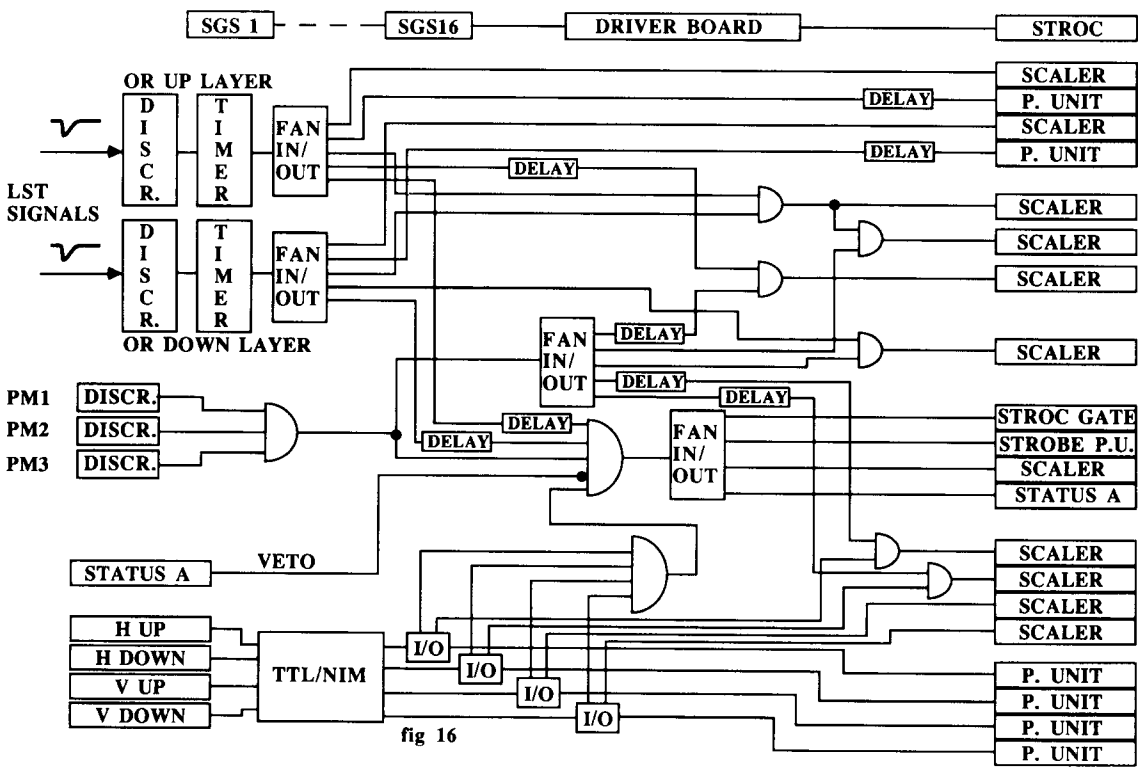

Fig. 16. The trigger selection logic adopted and the electronic setup.

the best ground configuration is achieved with a unique large plane for the horizontal and vertical strips. This is obtained for the bottom parallel strips and the upper transverse strips through the insulation planes described in the assembly procedures. For intermediate strips, the grounds of the transverse bottom layer and parallel upper layer are attached together. Fig. 14 shows the plateau from wires signal of one LST in different conditions: (a) with only one layer switched on, (b) both layers switched on; (c) with neighbouring LSTs switched off. No differences in count rate can be noted.

Using the capacitive electrode system to pulse the strips, it is very easy to verify, as part of the standard acceptance test of the assembled chambers, that one can reach a value of the reference electronic threshold as low as 25 mV without recording any pulses except those of the pulsed layer. The same test is also performed switching on only one layer of LSTs at a time. In a sample of 100 000 events collected for each chamber, no hits or, in some cases, very few randomly distributed hits on the strips corresponding to the layer not supplied are recorded. Finally the strip multihit distribution in one layer remains identical switching on and off the other layer (fig. 15).

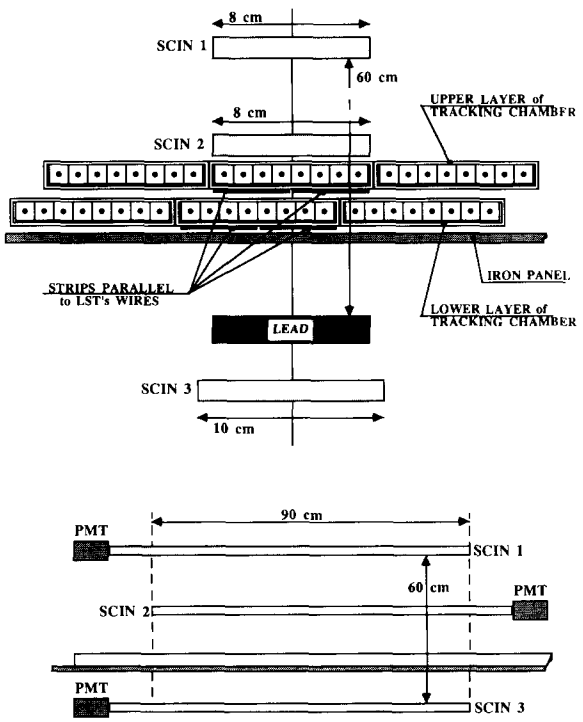

Fig. 17. The position of the telescope relative to the chamber (pos. A).

5.3. Strip readout performances

In order to characterize the LVD muon tracking system, its efficiency, resolution and uniformity have to be known. For this purpose measurements on individual chambers have been performed following the diagram already illustrated in figs. 10 and 11. The computer used in this case is a MaC-II. The trigger selection logic adopted and the electronic setup are shown in fig. 16. There are three main triggers: *Trigger A* is one of the four strip layer signals, H_{up}, H_{down}, V_{up}, V_{down}, described above or any combination of them (cosmic ray particles and low-energy radioactivity background are selected with this). *Trigger B* corresponds to passing-through particles; a threefold scintillator telescope selects tracks within $\pm 9°$ Φ angle measured in a plane perpendicular to the wires and a $\pm 56°$ Θ angle measured in a plane parallel to the wires. A lead absorber is put between the scintillators in order to cut the soft component of cosmic rays. *Trigger C* uses wire signals of a selected group of LSTs from any of the four layers of the chamber.

The acquisition software records all the necessary parameters, e.g., streamer tube high voltage, the respective X and Y threshold voltages, temperature, pressure, humidity. The contents of the STROC memory, as well as information from the trigger signal configuration coded on pattern units, are recorded event by event. The program also checks for the occurrence of an overcurrent condition. The decodification of the event cluster and the strip hit distributions are shown periodically. Data files are then transfered to a MicroVAX for detailed off-line analysis.

We have measured the efficiency of the chamber readout system, first using the telescope coincidence as the trigger. The efficiency is defined by the ratio of the number of events on which at least one hit is recorded on the strip area covered by the telescope to the number of trigger events.

The measurements are taken in two different positions of the horizontal panel: position A is near the front-end electronics, position B is near the high voltage side. The position of the telescope relative to the chamber is shown in fig. 17; the scintillator widths are such as to cover (laterally only) one LST in the upper layer and a portion of two LSTs in the lower layer in position A; the reverse, in position B. Fig. 18 reports the strip geometrical efficiency with respect to the cosmic ray trigger as a function of the reference value of the front-end electronics threshold. A wide full efficiency plateau is measured for the X- and Y-strips; the measured geometrical acceptance of the two layers of detectors is the one expected, taking into account the locally different numbers of nonsensitive PVC walls. The same value of acceptance has been obtained for the LSTs subtending the telescope when the wire sig-

nals are discriminated at a level of -10 mV/50 Ω: 92.5% for the upper layer and 89.9% for the lower one with the telescope in position A; 88.2% for the upper layer, 92.5% for the lower one in position B.

No sensible differences can be seen between the two different layers of detectors or between the two different positions, while a more rapid decrease in the efficiency of the transverse strips is observed. The strip readout efficiency has been also measured with respect to a C-type trigger obtained from the AND of the two layers of LSTs in a restricted portion of the horizontal plane. LST signals were discriminated at a level of -10 mV/50 Ω threshold. The efficiency measured as a function of the electronic reference threshold is

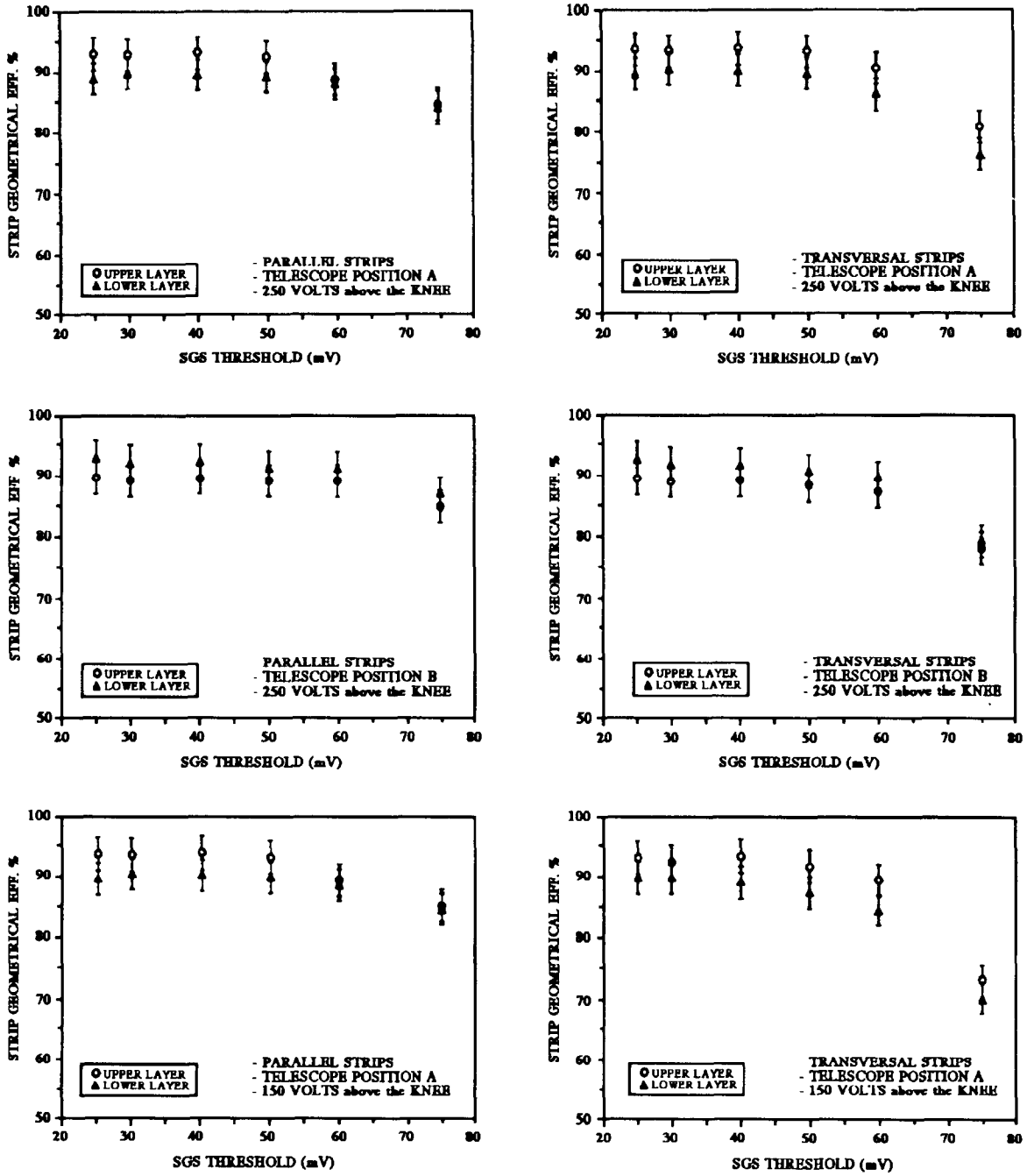

Fig. 18. The strip geometrical efficiency as a function of the reference electronic threshold.

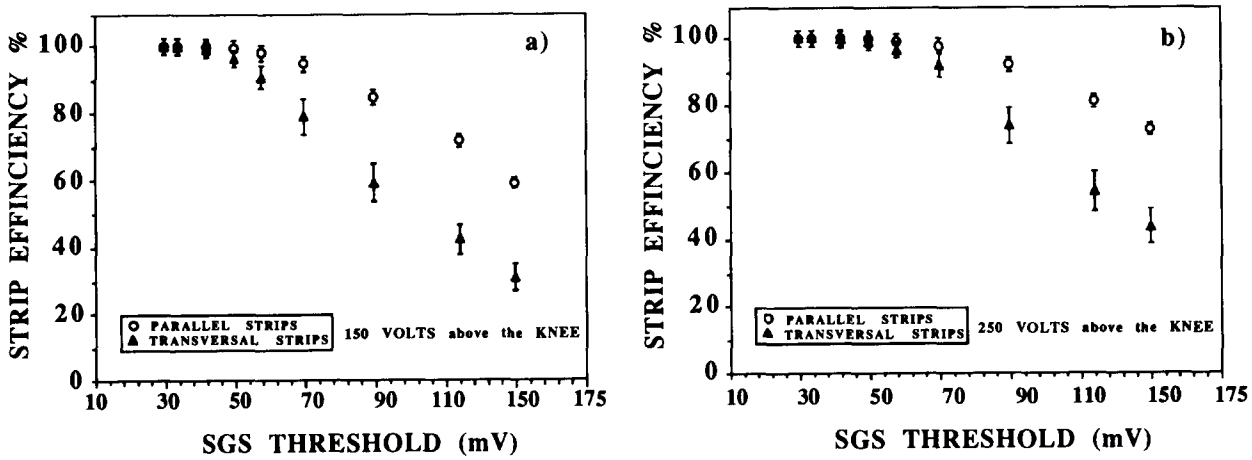

Fig. 19. The strip efficiency with respect to the LST signals.

shown in fig. 19a and 19b at an operating voltage of 250 V and 150 V, respectively, above knee position. In case (a), we have found an efficiency greater than 95% up to 85 mV for parallel strips and 70 mV for transverse strips.

We recall that the layers of X- and Y-strips placed on opposite sides of the LSTs, each subtend roughly one half of the total solid angle from the streamer and then equally share the total induced charge. Nevertheless, as already reviewed, the mechanism for signal propagation is completely different in the two cases. SLD and UA1 Collaborations [10,11] have measured the charge distribution of induced pulses on adjacent strips both for X- and Y-strips. Normalizing the distribution to the central strip, a very narrow shape is observed for X-strips and a broader one for the Y-strips. On this basis, not only we can expect a different cluster hit multiplicity (as we will see later) but we can also understand the different behaviour in the measured efficiency for X- and Y-strips, since we are performing a digital readout with voltage sensing electronics.

We have also measured the strip efficiency as a function of the HV, expressed as the difference with respect to the average position of the plateau knee (the result is shown in fig. 20) at a fixed reference threshold of 40 mV on the front-end electronics. Strip signals, both parallel and transverse, show the same behaviour of the LST wires signals as a function of the HV: a

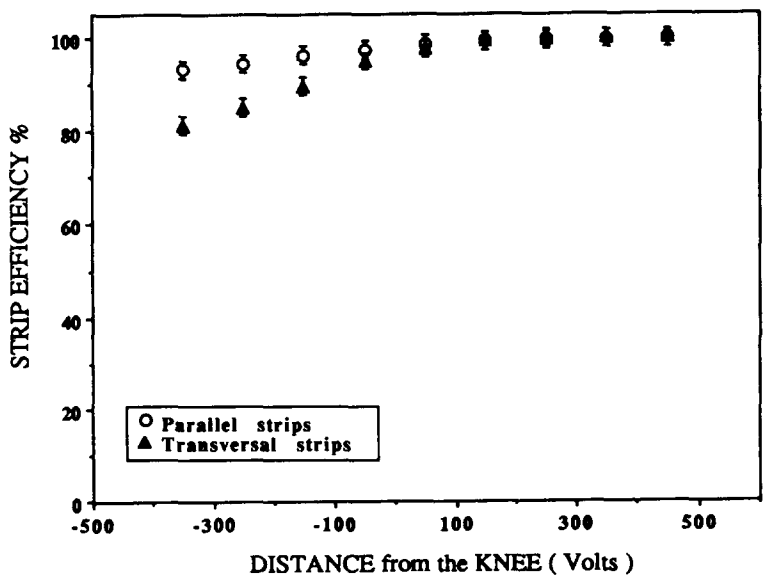

Fig. 20. The efficiency of strip readout as a function of the HV.

wide efficiency plateau in the limited streamer regime is obtained, while on the transition region between proportional and streamer, the characteristics of the front-end electronics are inadequate to guarantee, at this threshold, full efficiency.

In addition to the efficiency, a crucial point for the tracking system is the spatial resolution. For its evaluation we have measured the strip multihit as a function of the HV value and of the electronic threshold. The strip multihit, defined by the width of the event hit cluster, is shown in fig. 21 for parallel and transverse strips and for each of the four layers of detectors; the operating voltage of the LSTs is 100 V above the knee.

A perfect uniformity between the two layers is observed, while a higher multihit is found for vertical layers. This is easily explained taking into account the angular distribution of cosmic rays at surface level, which implies a higher probability that tracks cross

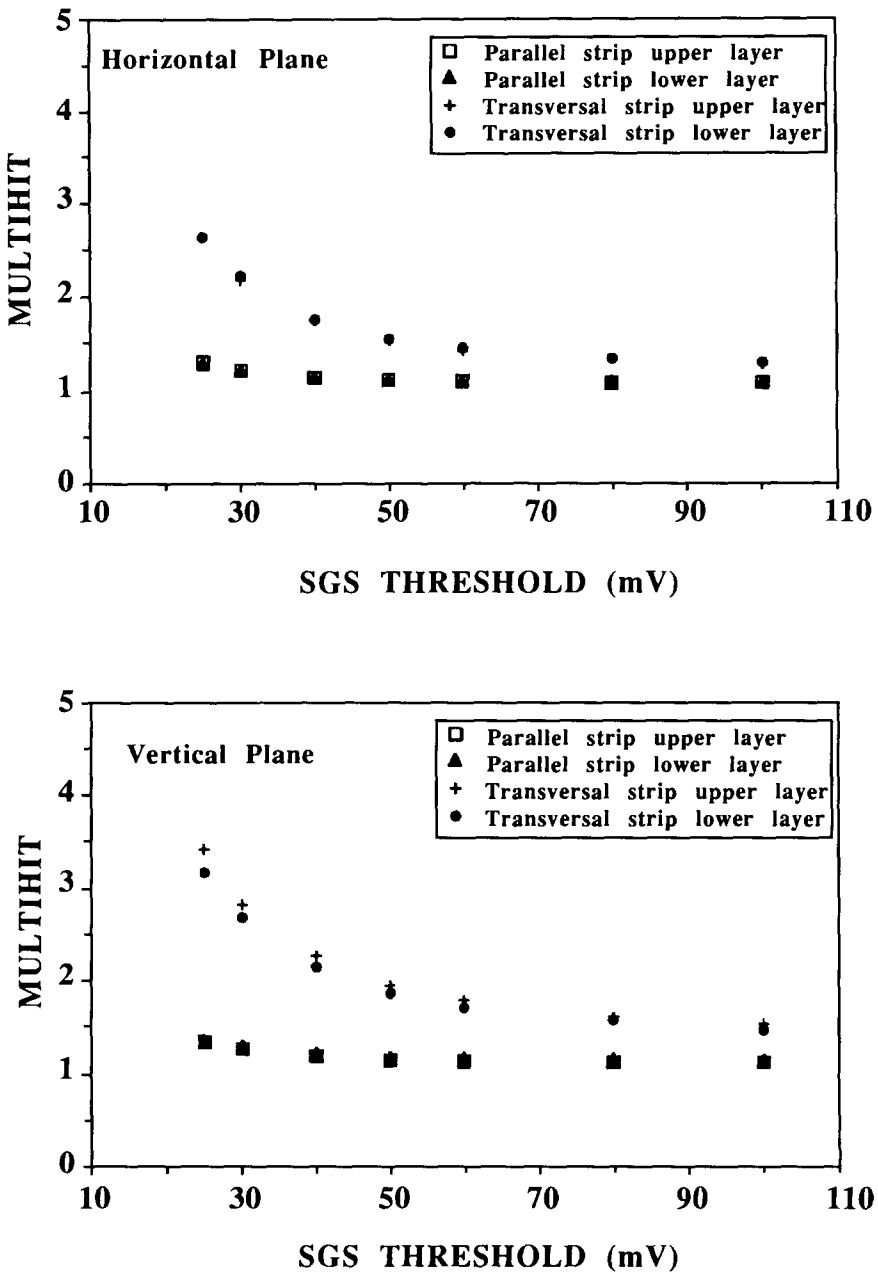

Fig. 21. The multihit distribution as a function of the electronic threshold.

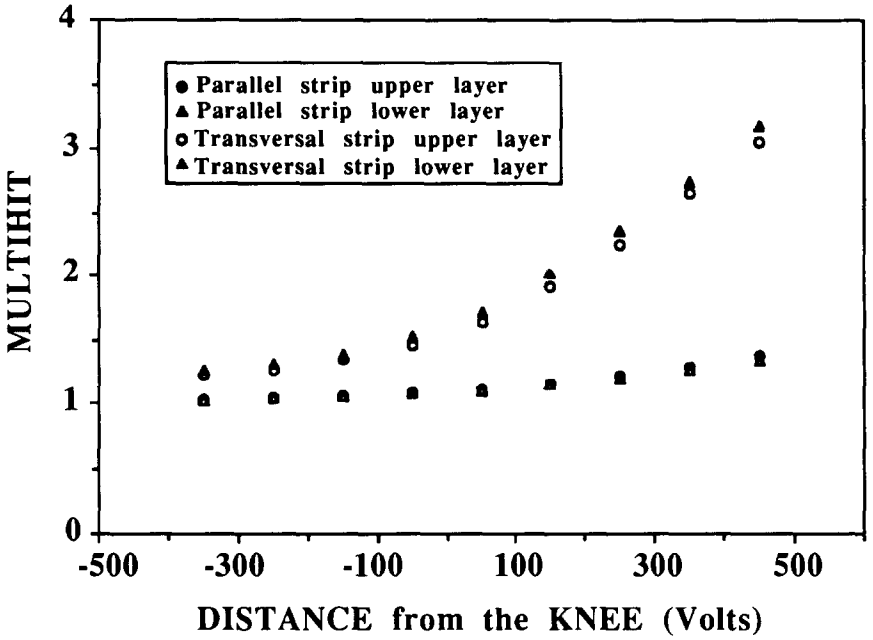

Fig. 22. The multihit distribution as a function of the HV.

more than one cell along the vertical panel than on the horizontal one. We can then consider the two distributions as the lower and upper limit for multihit measurement as a function of the crossing track angles. The multihit probability is also shown in fig. 22 as a function of the HV, expressed as distance from the plateau knee and at 40 mV for the reference electronic threshold. The correlation between strip efficiency and strip multihit is a key point in order to correctly choose the working point of the tracking system. From our measurements, we can conclude that, in order to guarantee full efficiency of the readout and at the same time maintain a reasonable multihit, a working point 100–150 V above the knee an electronics reference threshold of 40–50 mV seem the best operating ranges.

Finally, we investigated the spatial uniformity of the system. The hit distribution for X- and Y-strips along the chamber is shown for each one of the four layers in fig. 23a–f, triggering on the V_{up}, V_{down}, H_{up}, H_{down} signals. The distributions are measured at 150 V above the knee and for two different values of the electronics reference threshold, 30 mV and 80 mV. A very good spatial uniformity is observed also when the value of the threshold is increased. The effect of the higher Y-strip multihit can be again observed.

In tables 1 and 2, for completeness, we give the ratio of events with at least one hit on that layer with respect to the trigger events, as a function of the triggered layer, at the Frascati (LNF) surface level and in the Gran Sasso (LNGS) underground laboratory at 30 mV.

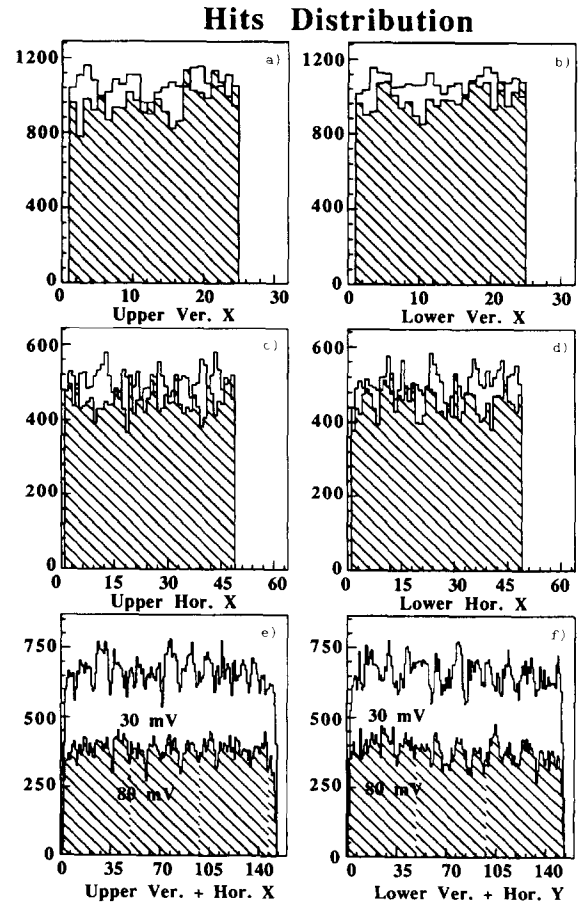

Fig. 23. The hit distribution along the chamber at two different values of the electronic threshold: 30 mV and 80 mV.

Table 1
Relative ratio of events for the layers of the chamber at the surface level

Trigger	LNF					
	H_{up}	Y_{up}	V_{up}	H_{down}	Y_{down}	V_{down}
H_{up}	0.99999	0.997	0.06	0.49	0.50	0.06
V_{up}	0.15	0.999	0.99997	0.15	0.34	0.32
H_{down}	0.50	0.50	0.06	0.99997	0.996	0.06
V_{down}	0.14	0.33	0.32	0.14	0.997	0.99997

Table 2
Relative ratio of events for the layers of the chamber in the underground laboratory

Trigger	LNGS					
	H_{up}	Y_{up}	V_{up}	H_{down}	Y_{down}	V_{down}
H_{up}	1.0	0.99915	0.0007	0.0062	0.0073	0.0010
V_{up}	0.0016	0.99910	1.0	0.0021	0.0067	0.0046
H_{down}	0.0072	0.0072	0.0009	0.99995	0.99910	0.0009
V_{down}	0.0017	0.0072	0.0055	0.0015	0.99915	1.0

6. Present status and quality uniformity of chamber production

The installation of the 38 tracking chambers belonging to the first tower has been accomplished in Hall A of Gran Sasso Laboratory and data taking has started. During chamber production, quality and acceptance tests were performed in order to guarantee stable and uniform performance of the whole system. The tests performed for this purpose were:

- gas leakage test of individual LSTs and of the whole chamber, as described above;
- LST wire count rate measurements;
- strip and readout electronics test pulsing with the capacitive electrode;
- cosmic ray data acquisition to check spatial uniformity and multihit distribution.

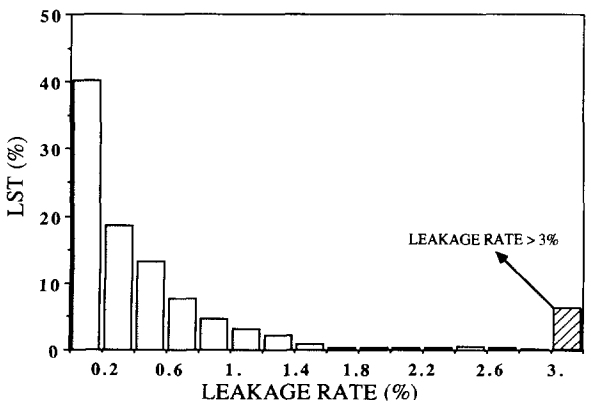

Fig. 24. Leakage rate distribution.

Fig. 24 shows the gas leakage rate distribution measured on individual streamer tubes. Tubes with leakage rate greater than 2% of the volume per day were repaired.

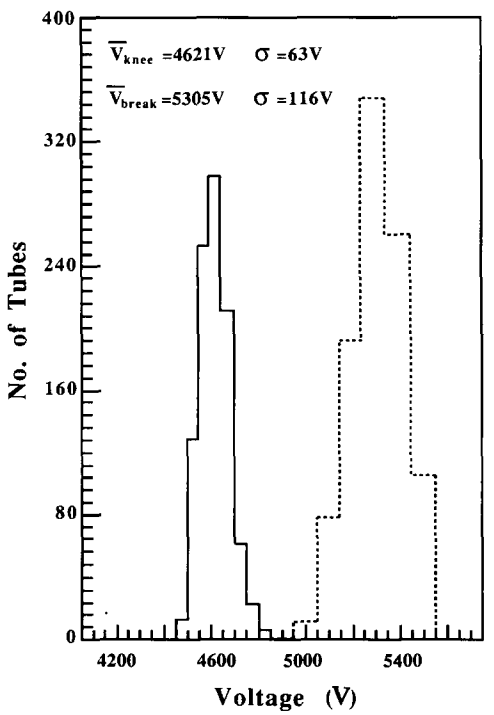

Fig. 25. Distribution of the voltages corresponding to the knee and the breakdown point.

Concerning the LST wire count rates, fig. 25 shows the distribution of the knee and breakdown position for a total of 12 chambers measured in homogeneous conditions, i.e. the same gas mixture and same end point voltage. Figs. 26 and 27 also show the distribution of the plateau widths versus slope and the percentage variation from the mean of the streamer tube count rates at a working operating voltage of 4800 V. The selection criteria ensure a plateau width not lower than 350 V and a variation of the count rate in the range (−12%)–(+15%). On average we have found that about 5% of the LSTs do not match the criteria, so they have been substituted.

The spatial uniformity of the whole detector can be seen in fig. 28, where the strip hit distributions for 7 wide chambers, at 4800 V, and at 30 mV for the front-end reference threshold, are reported. No systematic effects are observed, except for the distributions on the transverse strips. This could be explained by the presence of small dead zones at 50-cm intervals, due to the plastic bridges inserted in the LSTs to support the wires. Finally, fig. 29 shows the average multihit for the various layers for many chambers. A substantial uniformity is observed, with the variations mainly due to temperature, since all the measurements are taken at the same HV and front-end electronic reference threshold (4800 V, 30 mV). Again, the higher value for multihits on vertical chambers can be ob-

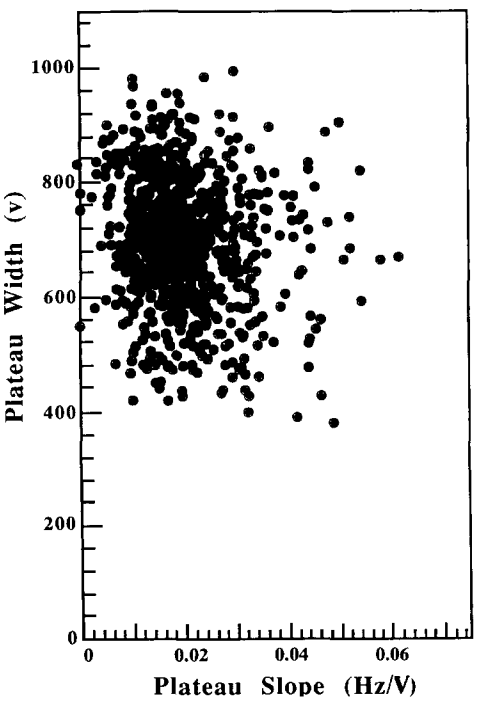

Fig. 26. Plateau widths versus slope.

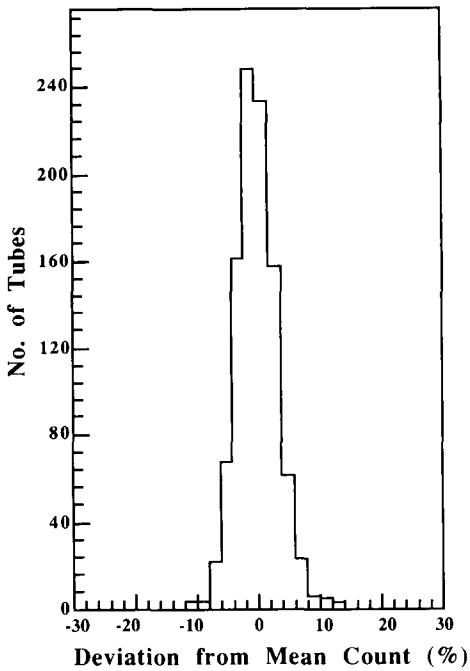

Fig. 27. Percentage variation of single streamer tube count rate.

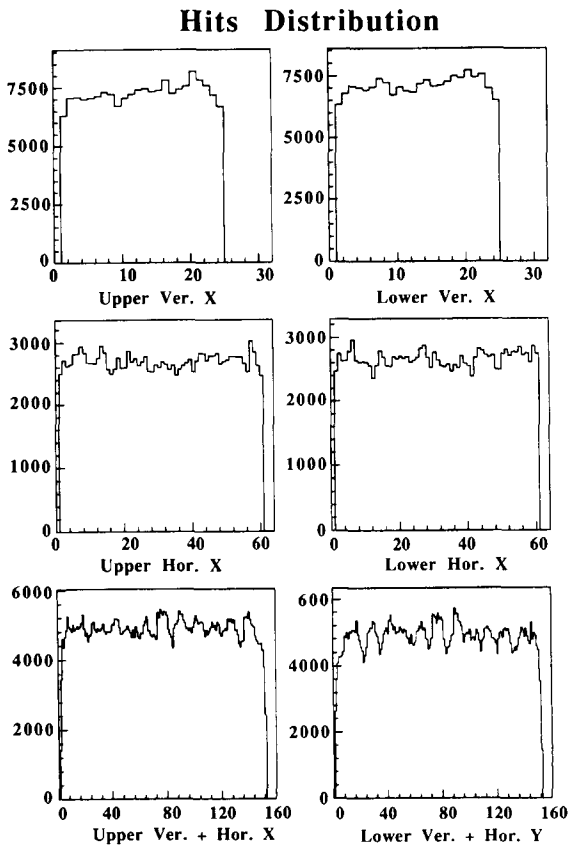

Fig. 28. Strip hit distributions for 7 chambers.

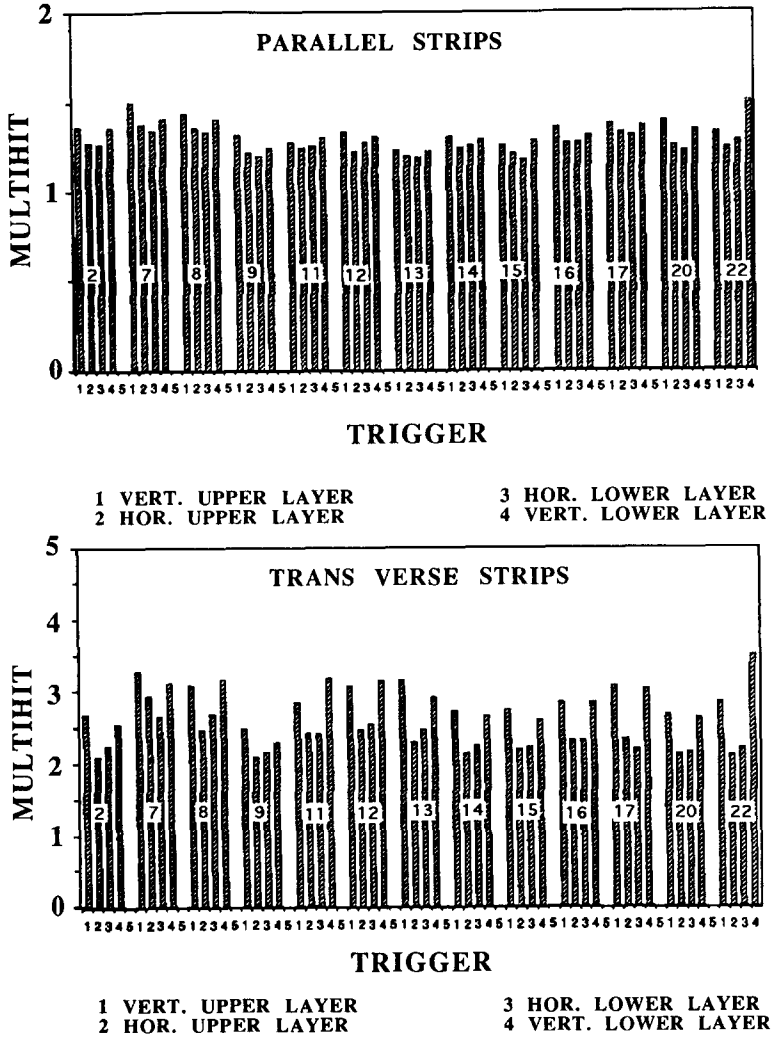

Fig. 29. The average multihit for the various layers of 13 chambers.

served; this systematic effect is not present, as expected, in the measurements taken at Gran Sasso.

Due to the modularity of the tracking system of the LVD experiment, individual chambers, as we have described, were assembled and tested at Frascati and then sent to Gran Sasso where, after the linkage to the scintillator detectors, they were installed in the apparatus. This procedure allows a considerable decrease in the time spent in the underground laboratory.

In the Gran Sasso Laboratory, situated at an altitude of ~ 900 m above sea level, we have found a displacement of 220 V (270 V expected) on the position of the knee of the LST single count rates with respect to the average value measured at Frascati. For completeness, table 3 gives the average count rate measured at the Frascati Laboratory and at the Gran Sasso Laboratory, for each of the four layers of one chamber.

Table 3
Average trigger rate

Trigger layer	Trigger rate at LNF [kHz]	Trigger rate at LNGS [Hz]
H_{up}	3.98	229
V_{up}	1.56	104
H_{down}	3.89	228
V_{down}	1.54	105

7. Conclusions

We have designed the tracking system of the LVD experiment and constructed the first tower. The main characteristics of the system, such as efficiency, spatial uniformity and resolution have been measured and found excellent. The design of the tracking chamber completely fulfils the requirements of the experiment.

A well defined and careful test procedure during chamber production has also ensured quality uniformity of the whole detector.

References

[1] C. Alberini et al., Nuovo Cim. 9C (1986) 237;
G. Bari et al., Nucl. Instr. and Meth. A264 (1988) 5;
G. Bari et al., Nucl. Instr. and Meth. A277 (1988) 11;
G. Bari et al., Proc. 3rd Winter School on Hadronic Physics, Folgaria, Italy, February 1988, eds. R. Cherubini, P. Dalpiaz and B. Minetti (North-Holland) p. 389.

[2] A. Zichichi, The Gran Sasso project, INFN/AE/82 (1982);
and E. Bellotti, Nucl. Instr. and Meth. A264 (1988).

[3] E. Pallante, Thesis, University of Rome "La Sapienza" (1989).

[4] E. Iarocci et al., Nucl. Instr. and Meth. 217 (1983) 30.

[5] G. Bari et al., Proc. 4th Topical Seminar on Experimental Apparatus for High Energy Physics and Astrophysics, San Miniato, Italy, May 90, eds. P. Giusti, F.L. Navarria and P. Pelfer (World Scientific) p. 468.

[6] G. Bari et al., LVD-LNF INT. MEMO 005 (1988).

[7] G. Bari et al., Proc. 4th Topical Seminar on Experimental Apparatus for High Energy Physics and Astrophysics, San Miniato, Italy, May 90, eds. P. Giusti, F.L. Navarria and P. Pelfer (World Scientific) p. 488.

[8] B. Alpat et al. LVD-LNF INT. MEMO 038 (1989).

[9] G. Battistoni et al., Nucl. Instr. and Meth. 176 (1980) 297;
and G. Battistoni et al., LNF-86/4 (P).

[10] A.C. Benvenuti, SLAC-PUB-4993 (1983).

[11] A. Bettini, UA1-TN 84-10 (1982).

[12] A. Gavestro et al., Nucl. Instr. and Meth. A312 (1992) 571.